J Solid State Electrochem (2002) 6: 513–521
DOI 10.1007/s10008-002-0276-5

ORIGINAL PAPER

A.G. Muñoz · M.M. Lohrengel

Kinetics of oxide growth and oxygen evolution on p-Si in neutral aqueous electrolytes

Received: 2 November 2001 / Accepted: 11 February 2002 / Published online: 30 April 2002

Abstract The growth of thin oxide films on wafers of p-Si, (100) orientation, was studied in neutral and acidic aqueous solutions up to 10 V by microelectrochemical (cyclic voltammograms and current transient of potential steps) and microellipsometric measurements. The oxidation occurs according to the high-field law with high-field parameters $\log(i_0/\mathrm{A\ cm^{-2}}) = -13.4 \pm 1$ and $\beta = 10.6 \pm 0.1$ nm $\mathrm{V^{-1}}$. The oxide films represent an almost ideal dielectric material with $\epsilon = 6.5$. Oxide growth is not affected by oxygen evolution, which starts at potentials > 3 V. The electron transfer process was analysed in relation to the oxygen evolution reaction. Owing to the presence of oxide thicknesses higher than 2 nm at this point, direct tunneling is less probable and a tunneling via traps should be assumed for the charge transfer. Evidence for coupled electronic and ionic conduction is presented. A contribution of the valence band in SiO_2 is stated for the corrosion of oxides at potentials > 4.5 V.

Keywords High-field growth · Silicon oxide · Oxygen evolution · Electron tunneling

Introduction

Thermally grown silicon oxide layers have been studied to a great extent during the last decades, owing to their importance for semiconductor technology. For this reason, methods for obtaining thin and high-quality oxide layers were developed in order to assess integrated circuit devices of smaller dimensions. The electrochemical oxidation of Si has become an alternative way to produce oxide layers at low temperatures, but most of the work in this field is focused on the characterization of the oxides obtained using different electrolytes and no precise mechanism has been proposed [1, 2, 3, 4, 5]. In addition, strong alkaline and acidic electrolytes were used for some studies, where enhanced corrosion at the oxide/electrolyte interface is expected. Oxide growth has also gained considerable interest in the area of Si surface etching, where dissolution in fluoride solutions occurs through a surface oxide film beyond the passivation potential. Oxide layers in the nanometer scale were made by means of scanning tunneling microscopy and growth mechanisms were proposed to reproduce the experimental behavior and to predict the oxide thickness obtained under different conditions [6, 7, 8]. However, the lack of precise potential control in these two-electrode arrangements prevents complete understanding of the growth mechanism and, hence, empirical factors must be introduced. In addition, the presence of an adsorbed layer of water, under which these experiments were performed, may lead to different surface conditions. There are some publications concerned with silicon oxide growth in non-aqueous electrolytes [9, 10, 11]. The effect of the presence of water and the ionic transport mechanism have been discussed. A rough linear logarithmic relationship between current density (c.d.) and field strength was first reported by Young et al. [10] in these media. However, these experiments were mainly performed under galvanostatic conditions. The oxygen evolution reaction on Si was scarcely studied or considered as a possible cause for a change in the oxide growth mechanism [1, 4]. The aim of this work is to obtain a better understanding of the growth kinetics of thin silicon oxide layers in neutral aqueous electrolytes at relatively low anodic potentials. For comparison,

A.G. Muñoz (✉) · M.M. Lohrengel
Institut für Physikalische Chemie und Elektrochemie
der Heinrich-Heine Universität Düsseldorf,
Universitätsstrasse 1,
40225 Düsseldorf, Germany
E-mail: amunoz@criba.edu.ar
Tel.: +54-291-4595182
Fax: +54-291-4595182

Present address: A.G. Muñoz
INIEC, Universidad Nacional del Sur,
Av. Alem 1253, 8000 Bahia Blanca, Argentina

studies were also performed in other aqueous solutions. The oxygen evolution reaction (OER) was analysed with reference to different charge transfer mechanisms, which may take place through the oxide film.

Experimental

Experiments were performed on p-Si(100) wafers with a resistivity of 5–11 Ω cm (doping concentration approximately 2×10^{15} cm^{-3}) under illumination (white light). The wafers were cleaned in an ultrasonic bath of acetone, isopropanol, methanol, and finally water. Prior to each experiment the samples were etched with 2% HF for 1 min in order to remove the air-formed oxide film. Electrical contact was made with an InGa eutectic on the rear of the sample. Electrochemical measurements were performed with a capillary-based droplet cell with a wetted area of 10^{-3} to 10^{-5} cm^2. Details of the cell set-up have been described elsewhere [12]. The glass capillary was placed at different sites of the sample by means of an *xyz* stage immediately before each measurement. The use of a capillary cell allows a large number of measurements to be started with good reproducible initial surface conditions. Small electrode areas reduce the ohmic drop limitations in studying the potentiostatic current transients.

A stream of N_2 was passed over the sample surface to maintain it in a dry atmosphere during the set of measurements. Even though illumination is not necessary in the case of p-Si, it simplified the cell control by the video microscope. A fine gold wire in the glass capillary served as a counter electrode. As a reference electrode, common Hg/mercury salt-based systems were used for the different electrolytes. Potentials were referred to the normal hydrogen electrode, in some cases versus a hydrogen electrode in the same solution (HESS) to make comparisons easier.

Capacity measurements were carried out with a lock-in system using an alternating sinusoidal potential wave with 1–3 mV amplitude and a frequency close to 1000 Hz. At this frequency the system is dominated by the dielectric properties of the oxide film and the real component of the impedance response was checked to be close to zero. Oxide thicknesses were measured ex situ by a microellipsometer with a HeNe laser as light source (632.8 nm) and compared with those calculated from electric charges. A three-layer media system with a homogeneous covering film was assumed. Then, the optical constants and the oxide thickness were determined by fitting the experimental spectrum [$\Delta(\lambda)$ and $\psi(\lambda)$] to the proposed model in the wavelength range 350 nm $< \lambda <$ 850 nm. Refractive indexes of $n = 1$ and $\tilde{n} = 3.879$–$j0.016$ ($\lambda = 632$ nm) for air and Si, respectively, were adopted (Spectra Ray, Sentech Instruments). Finally, the refractive index for SiO_2 was assumed to follow the Cauchy dispersion function $n = A_0 + A_1/\lambda^2 + A_2/\lambda^4$ and the extinction coefficient of the film was set to zero.

Current transients were recorded with an auto-ranging amplifier (range from amps to picoamps) with a time resolution of 10^{-6} s [13].

Results and discussion

Oxidation of the H-terminated surface

Figure 1 shows a cyclic voltammogram performed in acetate buffer of pH 5.9. Two anodic peaks can be observed at the initiation of the oxidation process. The first oxidation peak, which appears at approximately +0.2 V, corresponds to the oxidation of the hydrogen bonds present at the Si surface after HF treatment and, thus, the formation of a hydroxide layer (Eq. 1):

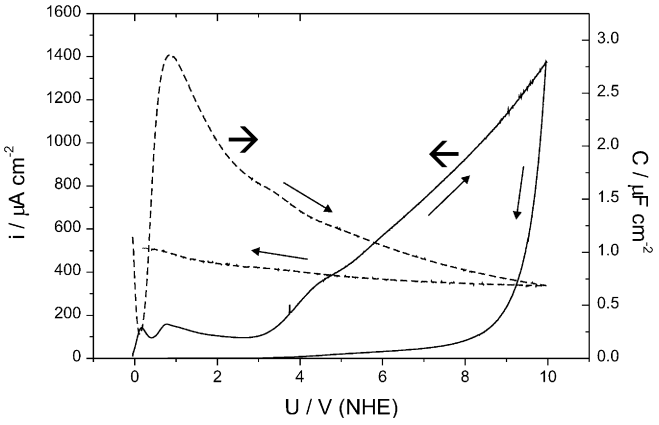

Fig. 1. Cyclic voltammogram and capacity obtained on p-Si(100) in acetate buffer solution (pH 5.9). $f = 1$ kHz, $dU/dt = 0.1$ V s^{-1}, $t = 25$ °C

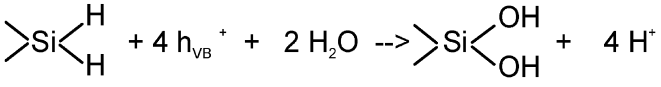

(1)

Under these conditions, no surface reconstruction was found [14]. Two dangling bonds must be considered and the calculated charge for their oxidation is 430 µC cm^{-2}, which corresponds to the charge obtained from integration of the first peak (450–550 µC cm^{-2}).

The second peak corresponds to the initiation of bulk oxide formation. No clear separation can be observed between these two peaks, so that no layer-by-layer growth may be here assumed. The formation of a hydroxide layer has been postulated as the first oxidation step from scanning probe microscopy [8]. The presence of a hydroxide film has also been claimed in the electropolishing of Si in fluoride-containing electrolytes [15, 16]. Thereafter, two OH groups react rapidly, giving rise to the first oxide monolayer by splitting a water molecule. At potentials higher than +1.5 V, a passive current is observed after the second peak up to +3 V. From this point, the anodic current increases due to the onset of the OER. Similar behavior has been observed by others in different electrolytes [3, 4].

Oxide growth mechanism

Neutral electrolytes

Figure 2a shows the potential dependence of the oxide thickness *d*, measured by microellipsometry, for potentiostatic and potentiodynamic growth. Linear relationships can be observed, typical for high-field oxide growth according to:

$$d = k(U - U_0) \tag{2}$$

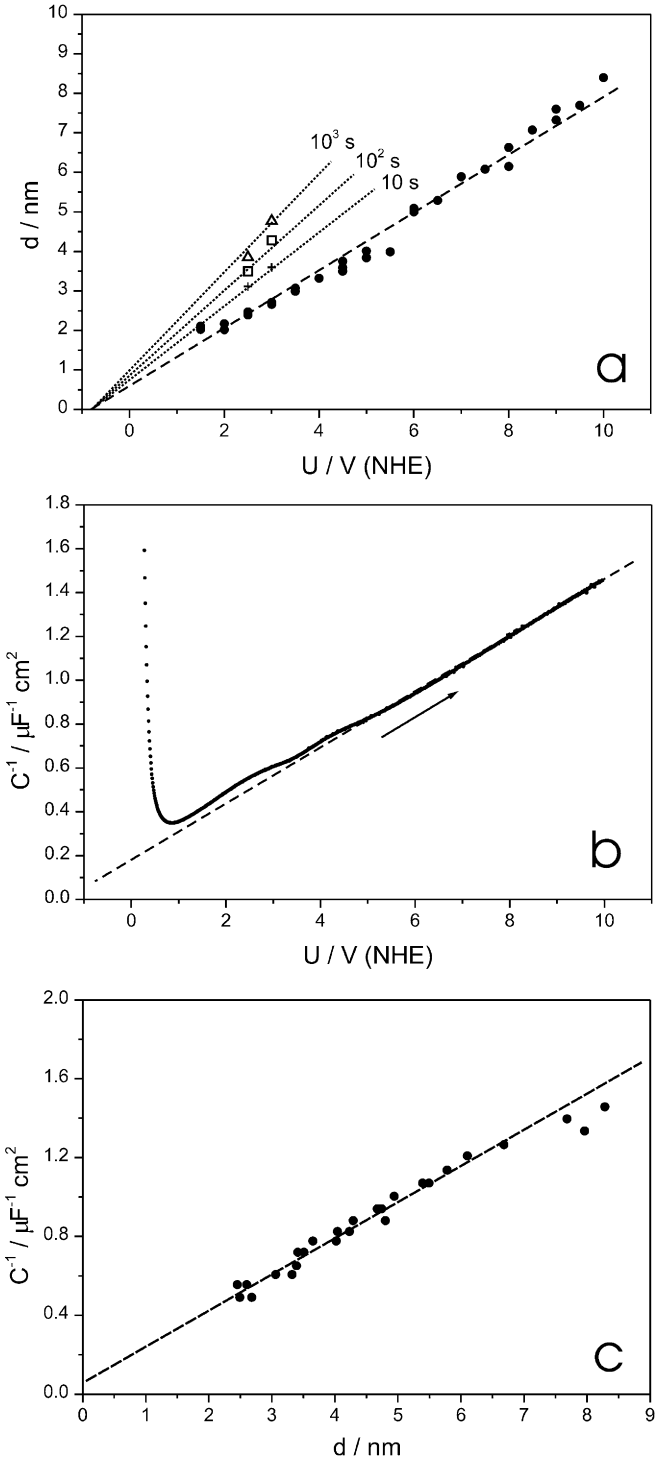

Fig. 2a–c. Potential-dependent oxide parameters in acetate buffer solution (pH 5.9) for potentiodynamic ($dU/dt = 0.1$ V s^{-1}) and potentiostatic growth. Thickness d obtained by microellipsometry (**a**), inverse capacity versus potential (**b**) from potentiodynamic experiments (1 kHz, $\Delta U = 1$ mV), and inverse capacity versus thickness (**c**) (data from **a** and **b**)

where k is the oxide formation factor. Extrapolation yielded a value of U_0 very close to the thermodynamic oxide formation potential of –0.86 V [17]. The formation factors depend on the growth conditions. Hence, different factors for potentiodynamic and potentiostatic growth are obtained: $k(100\ \text{mV s}^{-1}) = 0.74$ nm V^{-1}; k(pot 10 s) = 0.94 nm V^{-1}; k(pot 100 s) = 1.08 nm V^{-1}; k(pot 1000 s) = 1.26 nm V^{-1}.

The potentiodynamic k value is in accordance with those previously reported [18, 19]. The inverse of capacitance C^{-1} shows a more or less linear relationship with the potential (Fig. 2b), indicating linear growth without significant influence of the OER. The small hump at 2.5 V reflects the moderate changes of current (and therefore fluctuations of k) in this region. The extrapolation to $d = 0$ yields values of about 20 µF cm^{-2}, which is presumably the contribution of the interfaces, e.g. the space charge layer at the semiconductor's surface.

For a dielectric analysis, the inverse of capacitance C^{-1} was plotted versus the oxide thickness d measured by ellipsometry (Fig. 2c). The figure indicates that the oxide behaves, as expected, as an insulating dielectric material according to:

$$C^{-1} = d/\varepsilon\varepsilon_0 \tag{3}$$

with a dielectric number $\epsilon = 6.5$. This value is larger than 3.9 for thermal oxides [20], but similar to values found by others in alkaline electrolytes [3]. The presence of defects such as broken bonds and hydroxyl groups bonded as water or isolated silanols have been determined by spectroscopic techniques [21]. The presence of pores in the film is excluded from a pure high-field oxide growth.

Comparison with other electrolytes

Figure 3a shows the cyclic voltammograms performed on Si in different electrolytes. Only minor changes are observed in borate buffer of pH 8.4. On the other hand, a considerable enhancement of the OER occurs in H_2SO_4 solution in spite of a similar passivation current at potentials lower than 3 V. Moreover, the oxide capacities are much larger [e.g. 7 V: about 1.5 µF cm^{-2} (Fig. 4) versus 0.9 µF cm^{-2} at pH 6 (Fig. 1)], indicating a thinner film at small pH values, due to enhanced corrosion. Figure 3b shows the C^{-1} versus U plots obtained for the different electrolytes. No significant differences are noted for borate and acetate buffer solutions, where a linear relationship with identical slopes is observed in the whole potential region investigated. Similar behavior can be observed in H_2SO_4 only up to 4 V. From this point, a considerable deviation appears. Thus, remarkably, no influence seems to be exerted by anions during oxide growth in neutral solutions. The absence of incorporation of anions (PO_4^{3-}, SO_4^{2-}, $C_2O_4^{2-}$) into the growing oxide has already been suggested [22].

Figure 4a shows normalized cyclic voltammograms and the corresponding capacities in H_2SO_4 at different scan rates dU/dt (10 mV s^{-1} and 100 mV s^{-1}). Oxide formation and capacity up to 4 V are very similar,

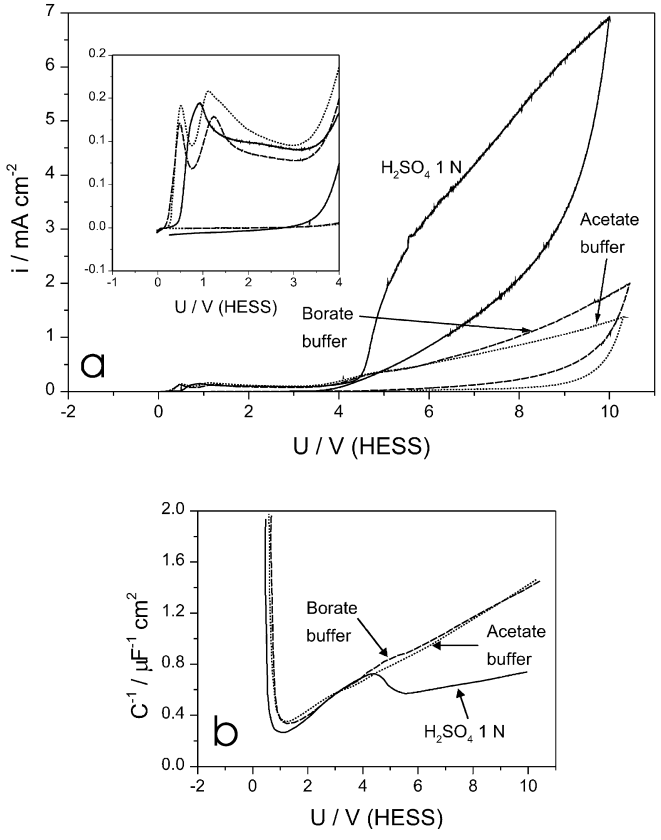

Fig. 3. **a** Cyclic voltammograms on p-Si(100) in different electrolytes. **b** Inverse capacity versus potential obtained for different electrolytes at $f = 1$ kHz

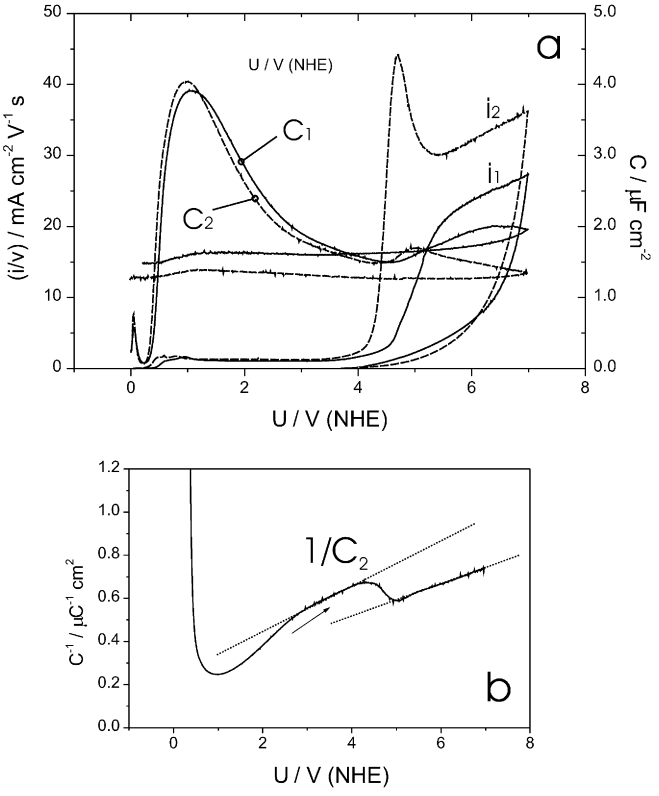

Fig. 4. **a** Normalized cyclic voltammograms (current divided by sweep rate) and capacity obtained on Si(100) in H_2SO_4 at different scan rates: 1: $dU/dt = 0.1$ V s^{-1} and 2: $dU/dt = 0.01$ V s^{-1}. **b** Inverse capacity to monitor the thickness changes ($dU/dt = 0.01$ V s^{-1})

indicating a weak dependence of the formation factor k on the sweep rate. However, they differ significantly during oxygen evolution. Ellipsometric measurements have shown a deviation towards smaller oxide thickness at this point.

The complex behavior can be better explained for $dU/dt = 10$ mV s^{-1}. The corrosion rate is small compared with layer formation below 4 V. At 4 V the potential drop at the interface oxide/electrolyte, $\Delta U_{ox/el}$, increases strongly. Therefore, the corrosion current i_{corr} increases as well and exceeds the oxide formation current i_{ox} at both sweep rates. Since the total potential drop remains constant, an increase of $\Delta U_{ox/el}$ means a decrease of the field strength E within the film. Thus, i_{ox} must also decrease according to the high-field equation:

$$i_{ox} = i_0 \exp(\beta E) = i_0 \exp[\beta(U_{ox} - U_0)/d] \quad (4)$$

where i_0 and β are oxide-specific constants. The corresponding thinning of the film is indicated by the current increase and the capacity maximum at 5 V. Thereafter, the potential and E increase until the ionic current in the film, i_{ox}, becomes larger than i_{corr}. Now, the oxide growth continues, but at a higher E within the film. This sequence can also be followed in the C^{-1} versus U plot (Fig. 4b). The slope decreases slightly at potentials > 5 V, indicating a higher dielectric number ϵ. A higher E during formation may lead to a different number of defects or incorporation of precipitated corrosion products. This, in turn, made it difficult to obtain reliable oxide thickness at $U > 6$ V by ellipsometry. At 100 mV s^{-1} the effects are similar but less pronounced, because i_{ox} is ten times larger and less influenced by the sweep-independent corrosion.

Below 3 V the capacity of the oxide film is larger than 2 μF cm^{-2} and therefore simple behavior according to Eq. 4 is not observed, because the capacity of the space charge layer in the silicon interface, connected in series, cannot be omitted.

Analysis of current transients

Current transients of potentiostatic pulse experiments on a previously formed oxide film (Fig. 5) were carried out to obtain deeper insight into the growth kinetics and to determine the high-field oxide constants (i_0 and β, Eq. 4). At times shorter than 10^{-4} s, a Debye charging process occurs, which can be simulated adopting a simplified RC model: oxide capacity and electrolyte resistance in series (dotted curve in Fig. 5, $R = 8\ \Omega$ cm^2, $C = 2.5$ μF cm^{-2}).

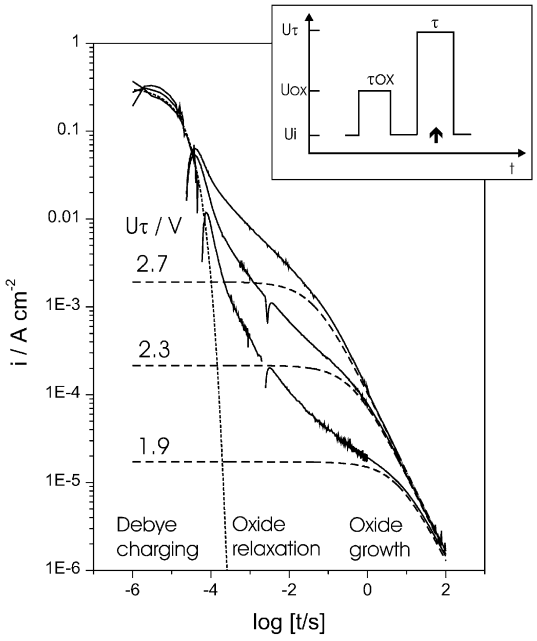

Fig. 5. Current transients of potentiostatic steps (to 1.9, 2.3, and 2.7 V) on previously formed thin oxide films (1.5 V, 100 s, $d_0 \approx 1.5$ nm) on p-Si(100) in borate buffer solution, pH 8.4. *Dotted line*: simulated Debye charging curve. *Dashed lines*: simulated oxide growth curves. $U_0 = -0.86$ V, $\log(i_0/\mathrm{A\ cm^{-2}}) = -13.4 \pm 1$, $\beta = 1.06 \pm 0.1 \times 10^{-6}$ cm V^{-1}

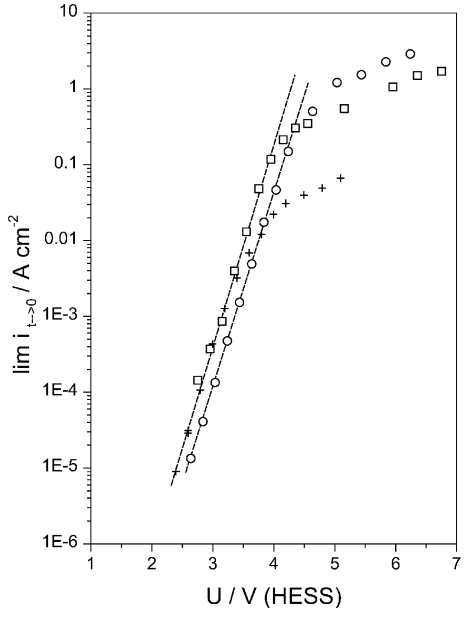

Fig. 6. Logarithm of initial oxide growth current obtained from transients in different electrolytes versus potential (HESS). *Crosses*: borate buffer, pH 8.4, $d_0 \approx 1.5$ nm. *Squares*: acetate buffer, pH 5.9, $d_0 \approx 1.7$ nm. *Circles*: 1 N H_2SO_4, $d_0 \approx 2.2$ nm

Then, the current decay observed between 10^{-4} s and 10^{-1} s is commonly attributed to dielectric relaxation processes within the oxide layer [23, 24]. The form of the curve may be explained in terms of a flat distribution function of relaxation times [25, 26]. Finally, the current reaches a linear relationship with a slope $d \log i / d \log t = -1$, this being typical for high-field oxide growth.

As common in solids, the ionic transport is explained by thermally activated, field-assisted hopping. Thus, according to this model, an exponential dependence of c.d. on E is predicted for $E > 10^6$ V cm^{-1} [10, 27] (Eq. 4). Assuming a current efficiency of 1 (no corrosion at pH 6), oxide growth is given by the differential equation:

$$\mathrm{d}d/\mathrm{d}t = (M/\rho_{\mathrm{ox}} zF) i_0 \exp[\beta(U - U_0)/d] \qquad (5)$$

which can be solved by numeric integration [24]. Together with Eq. 4, transients of pure high-field growth can be calculated, omitting other processes like Debye charging or dielectric relaxation. These transients are presented in Fig. 5 as dashed curves, showing a good correspondence with experiment at $t > 0.1$ s.

For short times, a linear relationship between $\log i$ and U is expected from Eq. 4, as long as $d = d_0$. The values of the initial growth currents cannot be directly identified as they are hidden by the relaxation processes. Therefore, they were taken as the intersection points of the linear parts corresponding to the relaxation and high-field growth.

Figure 6 shows the corresponding initial currents as a function of the pulse potential for various electrolytes. A good linear relationship is observed for currents < 0.1 A cm^{-2}. At higher c.d. values, deviations according to the ohmic drop in the electrolyte can be noted. From Fig. 6, resistances of about 1 Ω cm^2 (H_2SO_4), 3 Ω cm^2 (acetate), and 33 Ω cm^2 (borate) can be estimated, reflecting the different conductivities of the electrolytes: 77 mΩ^{-1} cm^{-1} (H_2SO_4), 24 mΩ^{-1} cm^{-1} (acetate), and 5.8 mΩ^{-1} cm^{-1} (borate). The analysis according to Eq. 4 yielded $\log(i_0/\mathrm{A\ cm^{-2}}) = -13.4 \pm 1$ and $\beta = 10.6 \pm 0.1$ nm V^{-1}. Further calculations, e.g. the current transient simulations in Fig. 5, were carried out with these parameters.

There is a displacement of 400 mV for the curve corresponding to H_2SO_4 compared with the other solutions. The c.d. values are smaller (approximately by a factor of 2), which means a lower mobility of the migrating species. It is accepted that the incorporation of anions from the electrolyte reduces the mobility of oxygen ions [24]. An increasing concentration of sulfate ions at the electrolyte interface because of the higher potential drop and the lower OH^- concentration may be assumed.

High-field-assisted ionic conduction has already been suggested by Young et al. [10]. However, the growth mechanism was a matter of discussion. A parabolic growth was reported in ethylene glycol based electrolytes at high anodic potentials [27] and a semi-empirical power law was proposed for oxides grown by a scanning force microscope [28].

The transport number of oxygen in silicon oxide was determined to be close to 1 and, hence, O^{2-} (or OH^-) should be the mobile species [1, 9, 29]. The factor $\beta = \alpha azF/RT$ from Eq. 4 is determined by the symmetry

factor α, the jump distance a and the charge number z of the hopping ion. Thus, assuming a symmetry factor $\alpha = 0.5$, a reasonable jump distance of 0.27 nm, in agreement with a previously informed value [10], is obtained for $z = 2$ in acetate buffer.

Oxide growth during oxygen evolution

In order to separate the oxide growth from the OE current during potentiodynamic scans, the oxide thickness was followed by capacity and ellipsometric measurements (Fig. 2). In a next step, the high-field growth was proved in a potential step experiment, using ellipsometry to measure the thickness. However, the change of thickness must be sufficiently large to obtain a good resolution with this technique. This means that large potential steps must be applied. It gives rise to large c.d. values ($>>1$ A cm^{-2}) at the start and a reliable potential control could be only expected for times >1 s.

Oxide films of 3 nm thickness were prepared by potentiostatic polarization to 1.5 V for 100 s. Then, potential steps to 6 or 8 V for different times were applied and the resulting thicknesses were determined. Figure 7 shows the inverse thickness as a function of log t. For times >1 s a linear relationship is found according to the inverse-logarithmic law, which is a good approximation of Eq. 5 at longer times [24]. Accordingly, values of $\beta =$ ca. 10.2 nm V^{-1} were obtained in acetate buffer.

Oxygen evolution

Ellipsometric and capacity measurements showed that the oxide growth is almost unaffected by the simultaneous OER in neutral electrolytes (Fig. 2c). Therefore, the oxide formation current beyond 3 V could be calculated. Figure 8 shows the OE current density, calculated as the difference of experimental and oxide formation currents.

Slopes of 690 mV dec^{-1} and 8.4 V dec^{-1} for the lower and higher potentials, respectively, were found. The cathodic sweep is characterized by an almost constant oxide thickness of 8 nm. In the beginning, down to 8 V, some further oxide growth can be expected (typically some percent). Oxide corrosion should be negligible during the complete sweep in neutral electrolytes.

A change of mechanism is observed at about 4.5 V, independent of sweep direction and oxide film. This fact may be related to an accumulation of holes at the oxide/electrolyte interface, as will be later explained.

The time dependence of the OER for a potential step was obtained by subtracting the oxide growth current from the total one for $t > 10^{-3}$ s, where dielectric effects are negligible (Fig. 9). This current shows the same slope of –1 as for oxide growth. This indicates that both processes are coupled to the field strength within the oxide. The same experiment was performed for different increasing potentials. Figure 10 shows the OE current taken for constant times and plotted as a function of $(U-U_0)^{-1}$, where a good linearity could be found. Taking into account that the oxide thickness follows the inverse logarithmic law (Eq. 6), a proportionality of OE current with d^{-1} can be deduced (Eq. 7):

$$d^{-1} = A - \beta^{-1}(U - U_0)^{-1}\ln t \quad (6)$$

$$\ln i(\mathrm{O_2}) = B + k/d = B + kA - k\beta^{-1}(U - U_0)^{-1}\ln t \quad (7)$$

Then, a value of $k = 1.82\times10^{-5}$ cm was estimated from Fig. 10.

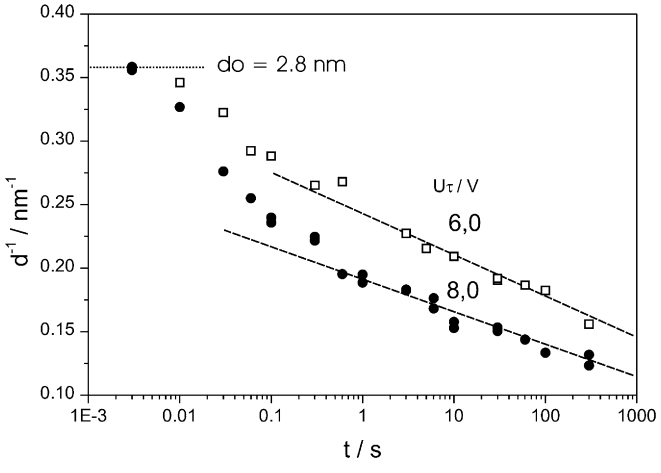

Fig. 7. Logarithm of the inverse of thickness versus log t obtained by microellipsometry for different potential steps; $d_0 \approx 3$ nm

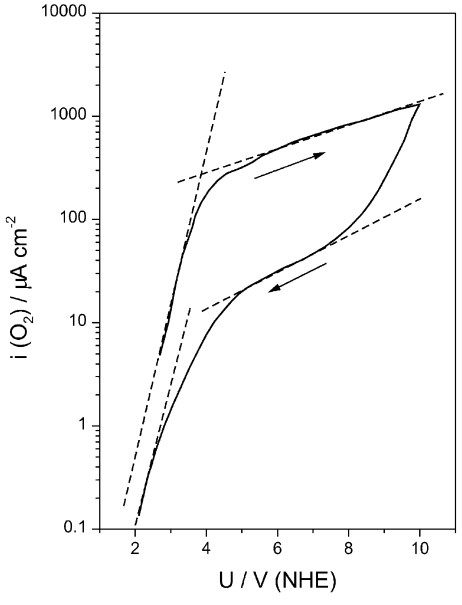

Fig. 8. Logarithm of oxygen current density versus potential obtained from potentiodynamic experiments by subtracting the oxide formation current from the total one

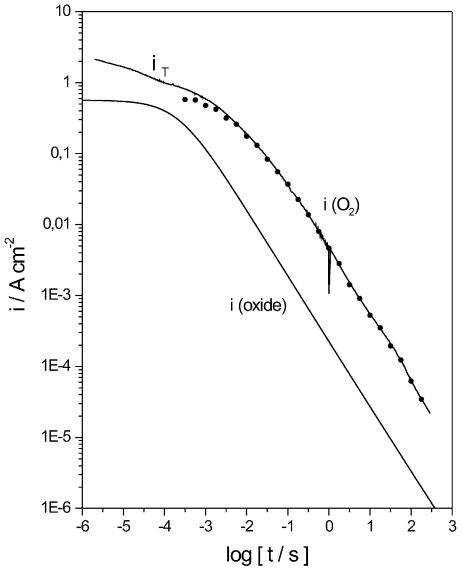

Fig. 9. Logarithm of current densities of oxide formation (simulated with $U_0 = -0.86$ V, $\log(i_0/\mathrm{A\ cm^{-2}}) = -13.4 \pm 1$, $\beta = 1.06 \pm 0.1 \times 10^{-6}$ cm $\mathrm{V^{-1}}$) and oxygen evolution versus logarithm of time, potential step to 8 V, initial thickness $d_0 \approx 3$ nm

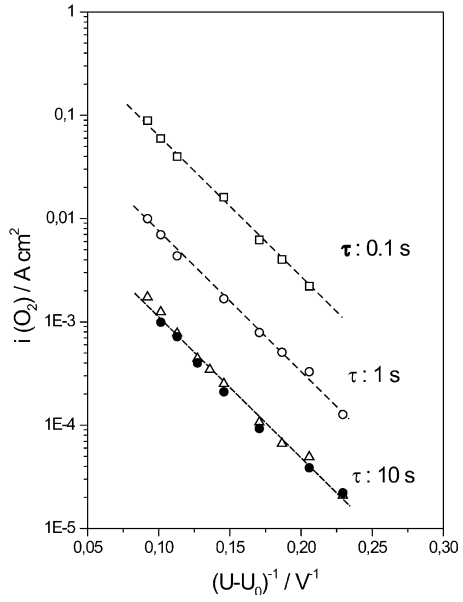

Fig. 10. Potential dependence of the oxygen evolution current for different constant times obtained from potentiostatic current transients performed on Si. Initial thickness (*open squares*, *circles*, *triangles*): $d \approx 2.5$ nm; (*filled circles*): $d \approx 1.7$ nm

Model

The charge transfer for the OER at oxide films is usually explained in terms of elastic and inelastic tunneling of electrons [30, 31]. The tunnel distances of about 4 nm at 4 V during the anodic sweep or 8 nm at the same potential during the cathodic sweep are too large to explain an electron transfer by direct tunneling. A resonance tunneling via electron traps within the band gap of the oxide film is more probable.

Different expressions for the c.d. were formulated, depending on the tunneling conditions [31, 32, 33]. Then, the influence of the thickness should be evaluated, since the OER occurs simultaneously with oxide growth. The following expression was proposed for elastic resonance tunneling, where electrons are transported from the electrolyte interface to unoccupied states at the metal [32]:

$$\ln(i/i_0) = -d'/d_0 + (U - U_0)Fd'/RTd \qquad (8)$$

where d' is the tunneling distance to the nearest localized state, d the oxide thickness, U–U_0 the potential difference inside the oxide film, and d_0 a constant. However, another dependence was derived from potentiostatic transient experiments. The direct relation between oxide growth and OE currents leads us to think about an influence of the applied field on the generation of traps.

Figure 11 depicts an energetic scheme of the Si/oxide/electrolyte system. For the interface Si/anodic SiO_2 we used some data from [5]: a valence band offset of 5.2 eV and no band bending in Si if it is oxide covered. To correlate the electrochemical scale, we assumed that the E in the oxide is zero at the thermodynamic oxide potential, i.e. –0.86 V. The Fermi level is located 0.3 eV [20] above the valence band and a reorganization energy of the redox system λ of approximately 1.2 eV was adopted. Then, OE becomes possible if the states of this redox system reach the energy of the Fermi level in Si at 3.3 V (or some 100 mV below). The electrons are transferred in a tunnel process at the Fermi level. At this potential, however, the oxide film thickness already exceeds 3 nm and the tunnel probability is too small. Thus, a sufficient number of states within the film must be assumed to enable resonance tunneling [30]. Tentatively, two quasi-bands are added: a *shallow band* according to the electron traps [5, 34] (two dotted lines in Fig. 11), and a *deep band* from deep traps 3 eV below the Fermi level, e.g. as reported elsewhere [34] (dashed line). The generation of new traps between these two bands should be also possible. Figure 11a illustrates an anodic sweep for 4 V ($d = 3.6$ nm) and 10 V ($d = 8$ nm).

At potentials < 3.1 V the Fermi level of the redox system shifts below the Fermi level in Si and oxygen evolution becomes impossible. At potentials > 3.1 V, two electron paths become possible: (1) direct electron tunneling from occupied terms in the electrolyte to the shallow band and movement to the silicon or (2) transfer to the deep band and direct tunneling at the Fermi level of Si.

The question of which one is favored depends on the shape of the Fermi level within the oxide, which is not known. With increasing potential, the number of occupied terms in the electrolyte, above the Fermi level of Si, increases as well. Accordingly, we find a relatively small β-factor of 690 mV $\mathrm{dec^{-1}}$ in this region. At about 4 V the distribution function of occupied terms is completely

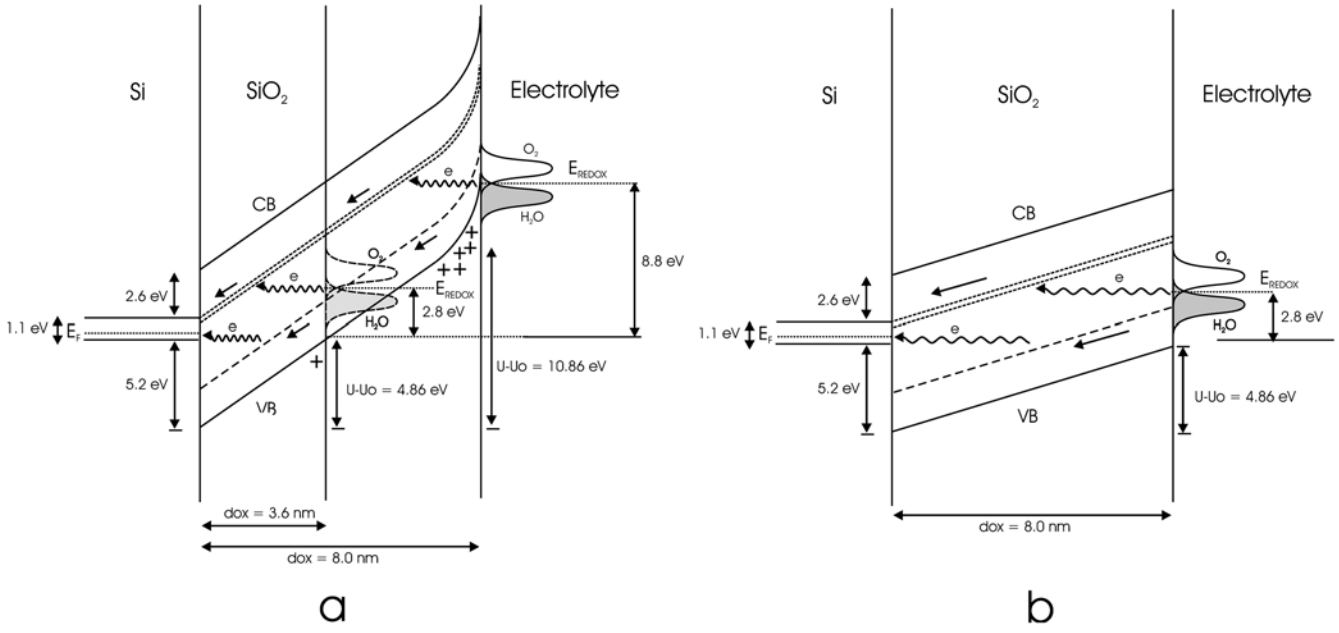

Fig. 11a, b. Band schemes of the system Si/SiO_2/electrolyte and distribution functions of the oxygen redox system. Anodic sweep (**a**) for 4 V ($d = 3.6$ nm) and 10 V ($d = 8$ nm) and cathodic sweep (**b**) for 8 nm oxide at 4 V

above the Fermi level in Si. At higher potentials (> 4 V) the tunnel distances remain constant and the process becomes almost independent on the potential, reflected by the large β-factor of 8.4 V dec^{-1}.

At 4.5 V, the valence band in SiO_2 comes close to the Fermi level in Si. Thus, holes are allowed to be formed in the valence band. They form a space charge at the interface with the electrolyte, increasing the potential drop and favoring the electron transfer. This, in turn, generates a deviation from the equilibrium of the protolytic reaction at the oxide surface (Eq. 9). Further reactions may conduct to the breakdown of Si-O back bonds and the formation of hydroxylated silicon compounds:

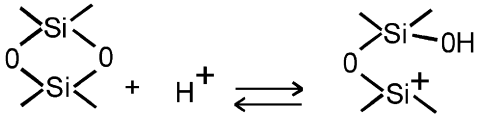

(9)

Thus, an enhanced corrosion rate can be expected in H_2SO_4 (Fig. 4) due to the high concentration of protons, which accelerates the hydroxylation process.

The change of mechanism at about 4.5 V is not influenced by the thickness. It takes place at both the cathodic and the anodic sweeps in spite of the change of thickness from 3.6 nm ($E = 13.5$ mV cm^{-1}) to 8 nm ($E = 6$ mV cm^{-1}). The slopes at potentials < 4 V are very similar and indicate the same mechanism (Fig. 11a and b). The tunnel distances, however, have increased by a factor given by the ratio 8 nm/3.6 nm. Therefore, the current decreased by almost one decade.

The excess charge of states within the oxide, required for resonance tunneling, might change the field strength. This is expected only if the number of them comes close to 10^{19} cm^{-3} [35]. Hence, it must be smaller. Values of 10^{17} or 10^{15} cm^{-3} seem to be more reasonable. A concentration of 10^{15} cm^{-3} may be just generated by the boron doping in the semiconductor. However, a mean distance of states of about 100 nm would be expected, if homogeneously distributed. Additional traps might be generated inside the oxide by applying high electric fields ($E > 7$ mV) [36]. Eventually, the density of these traps becomes high enough to lead to locally higher c.d. values. Then, the presence of boron impurities may be the cause for inhomogeneous trap generation and the appearance of preferential conduction paths. Therefore, the oxygen evolution must be concentrated to few sites or *hot spots*. The close relation between oxygen evolution and oxide growth may be thought in terms of traps generated during the transport of charged species.

Conclusions

According to the obtained results, the following conclusions may be addressed:

1. Capacitance and ellipsometric measurements show an almost ideal dielectric behavior of the oxide films in neutral and acid electrolytes up to 3 V. Owing to an accumulation of holes at the oxide/electrolyte interface, an enhanced corrosion was observed in H_2SO_4, when simultaneous oxygen evolution occurs.
2. The growth of Si oxide follows a high-field law in neutral electrolytes and the corresponding parameters were able to be calculated by analysis of potentiostatic pulses. This mechanism seems not to be affected by the oxygen evolution at potentials > 3 V.
3. A model for the charge transfer based on the tunneling of electrons via traps generated inside the oxide was presented. The influence of the field strength

on the generation of traps leads to a close correspondence between oxygen evolution and oxide growth.

Acknowledgements The financial support of the AGEF e.V. Institute at the Heinrich-Heine University of Düsseldorf and the Deutscher Akademischer Austauschdienst (DAAD) are gratefully acknowledged.

References

1. Bardwell JA, Clark KB, Michell DF, Bisaillion DA, Sproule GL, MacDougall B, Graham MJ (1993) J Electrochem Soc 140:2135
2. Bardwell JA, Allegretto EM, Phillips J, Buchanan M, Draper N (1996) J Electrochem Soc 143:2931
3. Schmuki P, Böhni H, Bardwell JA (1995) J Electrochem Soc 142:1705
4. Bardwell JA, Draper N, Schmuki P (1996) J Appl Phys 79:8761
5. Jungblut H, Lewerenz HJ (2000) Appl Surf Sci 168:194
6. Sugimura H, Nakagiri N (1995) Jpn J Appl Phys 34:3406
7. Avouris P, Hertel T, Martel R (1997) Appl Phys Lett 71:285
8. Gordon AE, Fayfield RT, Litfin DD, Higman TK (1995) J Vac Sci Technol B13:2805
9. Mende G (1998) Anodic oxidation of silicon as a low-temperature passivation technique. In: Campbell SA, Lewerenz HJ (eds) Semiconductor micromachining, vol. 2, chap. 9. Wiley, New York
10. Young L, Zobel FGR (1966) J Electrochem Soc 113:277
11. Jain GC, Prasad A, Chakravarty BC (1979) J Electrochem Soc 126:89
12. Lohrengel MM, Moehring A, Pilaski M (2000) Fresenius J Anal Chem 367:334
13. Lohrengel MM (1991) Principles and applications of pulse techniques to corrosion studies. In: Ferreira MGS, Melendres CA (eds) Electrochemical and optical techniques for the study and monitoring of metallic corrosion. Kluwer, Dordrecht, pp 69–121
14. Jaegerman W (1996) The semiconductor/electrolyte interface: a surface approach. In: White RE, Conway BE, Bockris JO'M (eds) Modern aspects of electrochemistry, vol. 30. Plenum Press, New York, p 87
15. Ozanam F, Chazalviel JN (1993) J Electron Spectrosc Relat Phenom 64/65:395
16. Chazalviel JN (1992) Electrochim Acta 37:865
17. Vetter KJ (1961) Elektrochemische kinetik. Springer, Berlin Heidelberg New York
18. Schultze JW, Lohrengel MM (2000) Electrochim Acta 45:2499
19. Pringle JPS (1979) Electrochim Acta 25:1423
20. Sze SM (1981) Physics of semiconductor devices. Wiley, New York
21. Clark KB, Bardwell JA, Baribeau JM (1994) J Appl Phys 76:3114
22. Parkhutik VP (1991) Electrochim Acta 36:1611
23. Rüße S, Lohrengel MM, Schultze JW (1994) Solid State Ionics 72:29
24. Lohrengel MM (1993) Mater Sci Eng R11:243
25. Jonscher AK (1977) Phys Status Solidi B 83:585
26. Pulfrey DL, Wilcox PS, Young L (1969) J Appl Phys 40:3891
27. Dignam MJ (1981) The kinetics of the growth of oxides. In: Bockris JO'M (ed) Comprehensive treatise of electrochemistry, vol. 4. Plenum Press, New York, p 247
28. Teuschler T, Mahr K, Miyazaki S, Hundhausen M, Ley L (1995) Appl Phys Lett 67:3144
29. Mackintosh WD, Plattner HH (1977) J Electrochem Soc 124:396
30. Schmickler W, Schultze JW (1986) Electron transfer reactions on oxide-covered metal electrodes. In: Bockris JO'M, Conway BE, White RE (eds) Modern aspects of electrochemistry, vol. 17. Plenum Press, New York, p 357
31. Schultze JW, Elfenthal L (1986) J Electroanal Chem 204:153
32. Schultze JW, Haga M (1977) Z Phys Chem NF 104:73
33. Schultze JW, Macagno VA (1986) Electrochim Acta 31:355
34. Yang BL, Wong H, Cheng YC (1996) Solid-State Electron 39:385
35. Lohrengel MM, Kluger K (1993) Elektrokhimiya 29:89
36. Dumin DJ (1997) Microelectron Reliab 37:1029